Photogrammetrie • Fernerkundung • Geoinformation 1/2005, S. 7–16, 10 Abb., 2 Tab.

Validated surface solar radiation inferred from NOAA-AVHRR and Meteosat-8 SEVIRI data

ANGELA SCHWIEBUS, ANNE LORENZ & FRANZ H. BERGER, Dresden

Keywords: remote sensing, cloud optical depth, solar radiation, NOAA AVHRR, Meteosat-8

Summary: The analysis scheme SESAT (**S**trahlungs- und **E**nergieflüsse aus **Sat**ellitendaten) was applied to NOAA AVHRR and Meteosat-8 data to calculate instantaneous values for solar radiation at surface. With the beforehand cloud classification 24 clouds can be discriminated along with the corresponding cloud optical thickness. For evaluation a comparison between the satellite-based results on the one hand and between NOAA data and ground measurements at 3 Anchor Stations on the other hand is presented. The obtained information supports a critical evaluation of the analysis results and demonstrates the capability of current remote sensing techniques.

Zusammenfassung: *Validierte Globalstrahlung am Erdboden bestimmt aus NOAA-AVHRR und Meteosat-8 SEVIRI Daten.* Das Analyseschema SESAT wurde für NOAA AVHRR und Meteosat-8 Daten angewendet, um Momentanwerte der Globalstrahlung am Erdboden zu bestimmen. Mittels einer Wolkenklassifikation, basierend auf der Maximum Likelihood Methode, können 24 Wolkenklassen und deren zugehörige optische Dicken unterschieden werden. Eine Validierung der Ergebnisse erfolgt durch den Vergleich der satellitenbasierten Ergebnisse untereinander und durch den Vergleich der NOAA Daten mit Bodenmessungen von 3 Ankerstationen. Die Validierung ermöglicht eine kritische Einschätzung der verwendeten Techniken hinsichtlich der erzielbaren Genauigkeit.

1 Introduction

The knowledge of surface energy fluxes provides important information for the study of regional and local aspects of the hydrologic cycle. Among the surface energy fluxes the radiation component is both the largest and the most controlling. Satellite remote sensing provides information about surface temperature and radiative properties at different temporal and spatial scales. The determination of radiative flux densities at surface is based upon these parameters, at the same time requiring first a correction of several atmospheric effects and second an accurate description of the interaction between clouds and radiation.

Regression techniques relating satellite data with ground measurements of solar radiation (TARPLEY 1979) were followed by physical approaches. There in general radiative transfer models like Streamer (KEY 1999) are used to analyze satellite data and to relate cloud microphysical and atmospheric properties with radiances measured at satellite level. Due to the lack of time and position adequate atmospheric profiles and information about the 3D geometrical structure of clouds and, with major importance, their optical and microphysical properties the accuracy of the radiation transfer codes is still limited. The uncertainty in cloud optical depth estimation is addressed by PINCUS et al. (1995) and ROZWADOWSKA (2004).

1432-8364/05/2005/0007 $ 2.50

However, smaller-scale cloud heterogeneities have greater impact on the radiative budget and must be accounted for. Numerous publications address the estimation of solar radiation from satellite data. PINKER et al. (1995) give an update of methods including a survey of global data sets like ERBE or ISCCP. Generally the parameterizations concerning cloud physics, atmosphere and aerosols became more sophisticated, like e.g. MASUDA et al. (1995), LASZLO & PINKER (1993), SCHMETZ (1993), CHOU (1997) or YUCEL et al. (2002) show. The achievable accuracy for satellite-based insolation was tested in a number of case studies. Inter model comparisons show errors around 10–20 Wm^{-2} on monthly time scale (PINKER et al. 1995). The validation with ground measurements yields RMSE up to 115 Wm^{-2} (e.g. BERGER 2001, TOVAR & BALDASANO 2001) for instantaneous and hourly solar radiation, respectively.

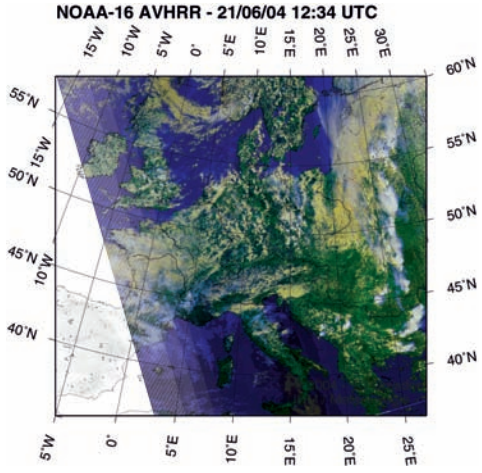

Fig. 1: NOAA-16 AVHRR color composite (channels 1, 2 and 4) for Europe for 21/06/2004.

2 Data

Satellite data with different spectral and spatial resolution were applied to derive cloud physical properties and solar radiation at surface. Results of NOAA16-AVHRR (Advanced Very High Resolution Radiometer) with a spatial resolution of around 1.1 km^2 at nadir (Fig. 1) are compared with Meteosat-8 SEVIRI (Spinning Enhanced Visible and Infrared Imager) owning a resolution of 3 km at nadir and about 4,5 × 3 km^2 for Central Europe. Meteosat-8 data were officially first released on January 27 in 2004. Due to NOAA offering only one overflight per day for the same area the comparison is limited to instantaneous values, not utilizing the high temporal resolution of Meteosat-8 (15 min).

The global digital elevation model GTOPO30 is additionally used to describe the underlying topography. It is based on data derived from 8 sources of elevation information hence the vertical accuracy of the GTOPO30 varies from 15 meters to 500 meters at 90 % confidence level. The horizontal grid spacing of the raster-structured data is 30 arc seconds (approximately 1 km). The vertical resolution was chosen with 1 m for NOAA and 25 m for Meteosat. The USGS EROS Data center offers GTOPO30 as public domain data.

3 Methods

The respective similar spectral charac-teristic of the considered channels (Tab. 1) allows to apply the same approach for both satellites. SESAT (BERGER 1995, 2001) is a modular analysis scheme to calculate radiant and energy flux densities at TOA and at surface. It was extensively tested for several periods and regions with NOAA AVHRR data (BERGER et al. 2002). The modular structure of SESAT permits the mo-

Tab. 1: Definition of the utilized spectral channels of NOAA and Meteosat-8.

	Band [µm]	channel	Band [µm]	channel	Band [µm]	channel
	visible		visible		thermal IR	
AVHRR	0,58 - 0,68	ch1	0,725 - 1,00	ch2	10,30 - 11,30	ch4
SEVIRI	0,56 - 0,71	ch1	0,74 - 0,88	ch2	9,80 - 11,80	ch9

dification of its single parts to the characteristics of SEVIRI. These adjustments mainly refer to the definition of new thresholds for brightness temperature and spectral reflectance and a normalization of tropopause temperature both required only for cloud classification.

The SESAT modules which are relevant for this paper are shortly explained below.

Module A:
The data are calibrated, geocoded and transformed onto a stereographic projection. The geocoded NOAA orbits allow the processing of time series due to the co-location of the single scenes. The instrument calibration usually is the linear type for the visible channels of both satellites

$$A = SC + I$$

where for NOAA A is the spectral albedo [%], S the slope (% albedo per count), C the satellite signal in 10 bit counts and I the intercept. The valid coefficients are updated by NOAA (NOAA KLM User's Guide 2000). For Meteosat-8 the above relation is defined with A the radiance $[\mathrm{mWm^{-2}sr^{-1}(cm^{-1})^{-1}}]$. The calibration coefficients (S, I) of Meteosat-8 SEVIRI channels are obtained from the repeat cycle prologue of each image (Eumetsat 2003). To build comparable conditions for insolation the visible channels were normalized with the solar zenith angle.
The infrared channels for Meteosat are calibrated with the MSG Data Manager (Taylor 2003). Then brightness temperature is assigned to the greyvalues (0-255) using a look-up table. For NOAA their data service (NESDIS) has generated look-up tables relating blackbody temperature to measured AVHRR radiance for each thermal channel covering a range of 180 K to 340 K.

Module B:
The test classes for the cloud classification are assessed based on physical albedo/temperature characteristics. Reflectance at 0,8 µm, normalized with the solar zenith angle for each pixel, and the brightness temperature at 10,8 µm are used for the determination of the test classes. The thresholds for the classes base on Berger (1995). For land and sea surfaces (class 1 to 4) a minimum decision rule for the reflectance and a maximum decision rule for the temperature are applied. For thick convective clouds (class 24) a maximum for albedo and a minimum temperature are chosen. For low and mid-level clouds the surface temperature was reduced depending on season to achieve the minimum temperature followed by a maximum decision for reflectances at the defined temperature. Altogether 24 classes, 4 cloudless and 20 cloud classes are obtained. Fig. 2 exemplary shows the assigned thresholds, where the single branches represent clouds in different heights. The corresponding cloud classes are listed in Tab. 2. Multilayered clouds are placed between the branches.

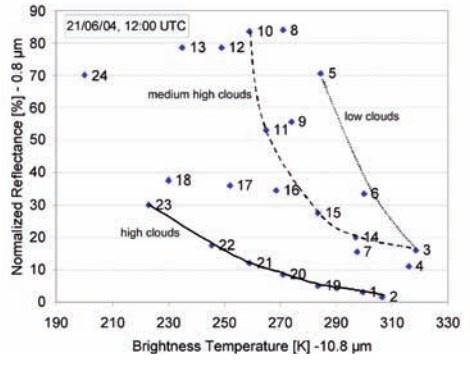

Fig. 2: Reflectance (0,8 µm) versus brightness temperature (10,8 µm) as basis for cloud classification. Tab. 2 contains the corresponding cloud classes.

Tab. 2: Definition of cloud classes.

Number	Description of cloud class
1 - 4	Land/ Sea/ Snow/ Sunglint
5	Low and thin
6, 7	Low and thick
8, 9	Multilayered I
10	Medium high and thick
11	Medium high and thin
12, 13	Multilayered II
14 - 16, 19 - 21	High and thin
17, 18, 22, 23	High and thick
24	Thick convective

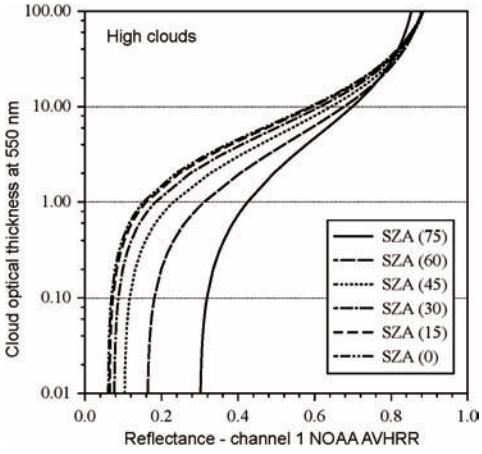

Fig. 3: NOAA-16 channel 1 reflectance at TOA versus optical depth for high clouds above a water surface and different solar zenith angles.

The cloud classification is carried out using a maximum likelihood classifier. For classification the 0,6 µm channel is additionally considered. The single training areas are detected automatically for the appropriated test classes. If a defined value for a class was found the 3 × 3 pixel neighbourhood is used to calculate the statistics for the maximum likelihood classification (mean value and covariance matrix). If no training area was found for a class, the statistics are provided.

Module C:
Cloud optical depth is achieved applying an inverse look-up table method. Radiative transfer simulations of outgoing radiance were performed using the 1D model Streamer (Key 1991) within the visible spectrum varying the most controlling parameters like solar zenith angle (SZA), satellite viewing angle, relative azimuth angle between sun and satellite, atmosphere type (humidity and aerosol conditions), and land surface type as well as optical depth itself. The results of these simulations are tabulated. Inversely the comparison between predicted and measured signal allows the determination of optical depth for nearly all appearing conditions. An example is shown for high clouds above a water surface (Fig. 3). The nonlinear relation between the integrated spectral reflectance and optical thickness is exemplified for varying SZA. Because it is harder to distinguish different reflectances at optically thick clouds the accuracy decreases for these cases (Pincus et al. 1995, Berger 2001).

Module D:
The determination of various land surface characteristics includes the spectral integrated surface reflectance (Song & Gao 1999) and the effective surface temperature (McClain et al. 1985) under different atmospheric conditions.

Module F:
Insolation at surface is derived inversely basing again on look-up tables obtained from broadband radiative transfer simulations. The inclusion of topography accounts for the effect of higher direct and lower diffuse radiation with increasing altitude. Reflected shortwave radiation and longwave components are calculated using the parameters determined in the previous modules.

4 Results

The following results cover only Europe although the processing of the complete Meteosat-8-scanned disc is intended. Problems occurred especially for the cloud classification over desert areas due to their ambiguous spectral properties, and for the latitude dependent differences for temperature and reflectance.

Fig. 4 shows the results of cloud classification for one exemplary date (Fig. 1 shows the color composite). The cloud structures for both NOAA and Meteosat match very well, whereas there are differences for the assigned cloud classes caused by differing thresholds for reflectance and brightness temperature when defining the test classes (Module B). The spatial integration of Meteosat blurs smaller structures which reduces reflectance and increases temperature. Meteosat data yield e.g. higher amounts of low thin clouds (yellowish, class 6). The areas with high thick and convective clouds

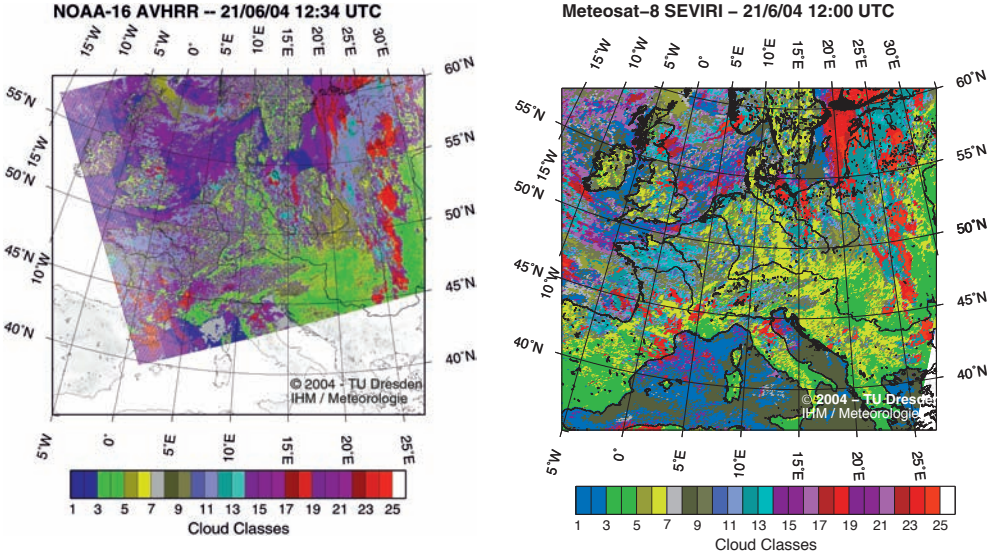

Fig. 4: Exemplary results of cloud classification for NOAA (left) and Meteosat (right) for 21/06/2004. Tab. 2 contains the corresponding cloud classes.

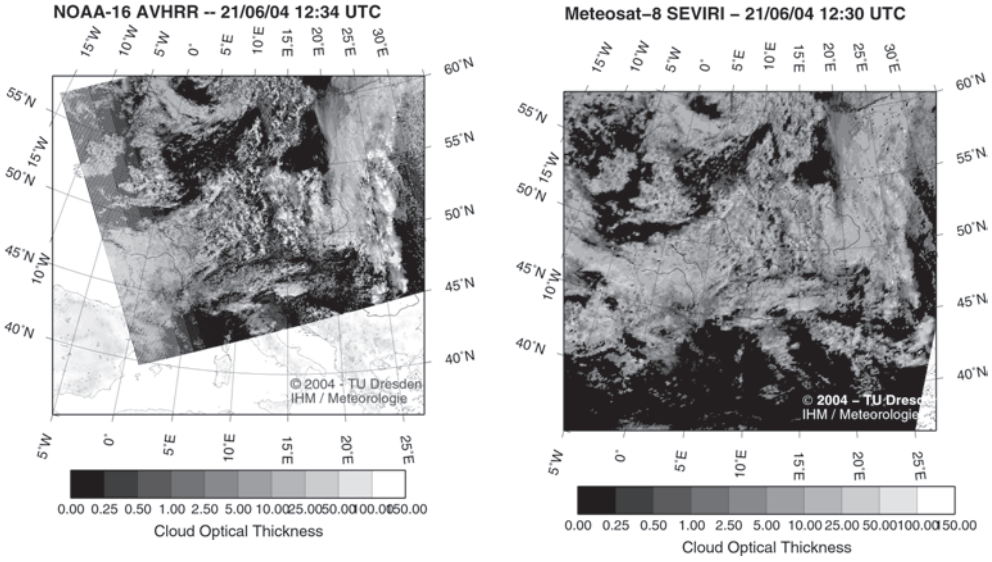

Fig. 5: Exemplary results for optical depth for NOAA (left) and Meteosat (right) for the same date.

(red, classes 17, 18, 22–24) are less extended for NOAA data, where only the centres of the high clusters are classified as thick or convective, whereas for the outer zone of these clusters thinner clouds are assigned. This shift toward thicker cloud classes in Meteosat classification exists throughout all classes. Related to the spatial resolution of Meteosat a coarser covariance matrix for the classification is generated causing this 'overestimation'. Cloud classification basically is a result by its own, it merely helps to provide information for the assignment of microphysical properties related to cer-

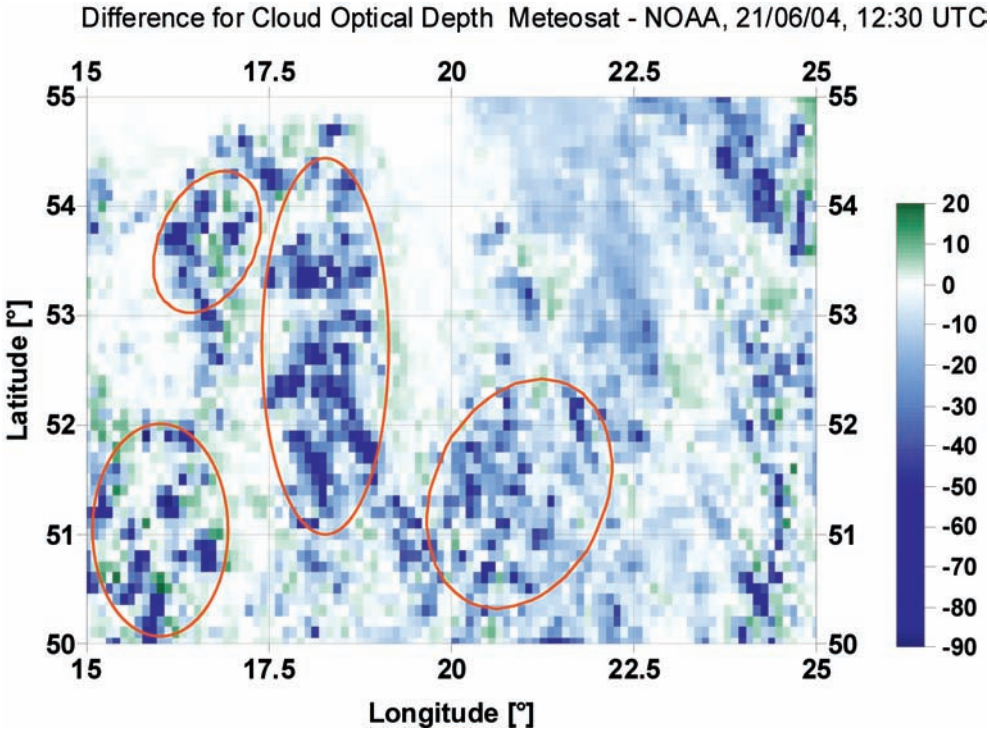

Fig. 6: Difference plot of cloud optical depth for 21/06/2004, 12:30 UTC for the area 15–25°E, 50–55°N. Regions with thick and multi-layered clouds are encircled in red.

tain cloud classes. An evaluation of classification results is difficult due to lack of references. The impact of uncertainties on the accuracy of adjacent parameters like cloud optical thickness is only secondary.

There are also differences between NOAA and Meteosat results for cloud optical depth τ (Fig. 5). Due to the coarser spatial resolution of Meteosat convective and small scale cloud structures are not detected in the very detail. Therefore these structures, owning very high optical thickness between 50 and 100, come out more clearly within the NOAA data. Mostly the cloud optical depth is lower for Meteosat caused by its spatial resolution (quite in opposite to the cloud classification result). The difference plot for a selected area with mainly thicker clouds (Fig. 6) shows such regions in blue colors. The high deviations (red circles) of up to 70 only appear for certain cloud classes, especially multilayered and thick types. The well-known effect of higher uncertainties towards large τ shows here very clearly.

The evaluation is problematic since none of the data may be regarded as the truth. Therefore also a numerical correction would not be appropriate. Estimates of cloud optical depth inferred from ground measurements like Rozwadowska (2004) shows are rare. In general both measurement uncertainties at satellite sensors and model parametrizations have a part in the uncertainty of cloud optical depth. Due to different sensor characteristics and calibration the uncertainty varies considerably between different satellites (Pincus et al. 1995). That is also the case for this analysis, whereas atmospheric model uncertainties should be negligible for the *comparison* of τ_{Meteosat} and τ_{NOAA} on account of using the same look-up tables.

The derived insolation at surface in Fig. 7 visually agrees well. Meteosat data show lower results, but the differences within the

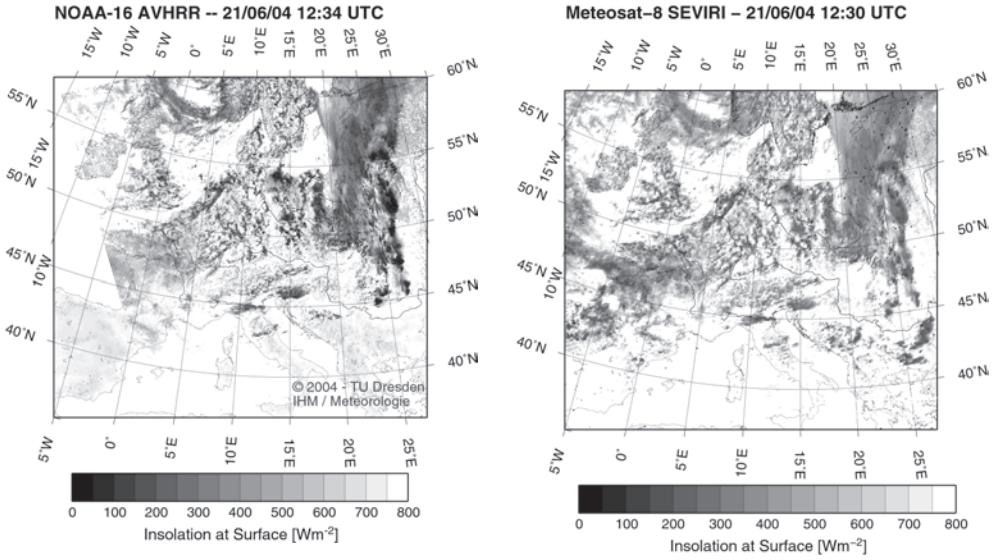

Fig. 7: Exemplary results for insolation at surface for NOAA (left) and Meteosat (right) for 21/06/2004.

cloud classification result and optical depth seem to have a minor impact here. The structures as well as the reduction of insolation for thick cloud structures are displayed well.

Fig. 8 plots the comparison of the satellite-based results of insolation at surface for June 21st. It contains about 4500 data points covering a region of 15° to 25°E and 50° to 55° N where cloud structure is very inhomogeneous at this time (mainly thick and convective types, partly cloudless). That may be the reason for the enormous scatter within the data. The RMSE for the shown example is 108 Wm^{-2}. The effect of lower Meteosat optical thickness as explained above is mirrored in the difference plot (Fig. 9) where the green pixel indicate higher insolation for Meteosat mostly in the range of 150–250 Wm^{-2}. For cloudless cases (blue pixels) NOAA insolation is higher since for Meteosat these regions are classified with low thin clouds. These values are shown in Fig. 8 as the rather horizontal branch in the upper part.

In former studies (Schwiebus 2004) the validation for insolation with ground truth data was carried out. Fig. 10 shows a comparison of NOAA insolation results with measurements of 3 Anchor Stations (Thaerandt, Melpitz, and Lindenberg; 10 × 10 pixel mean) using discrete cloud classes. The blue fit represents cloudless cases, the grey fit high and thick cloud cover. The following effects become apparent: for thick clouds with an optical thickness > 20 the cloud structures are uniform and the their impact on insolation is equally so the RMSE (Wm^{-2}, see table) is lower for such cloud

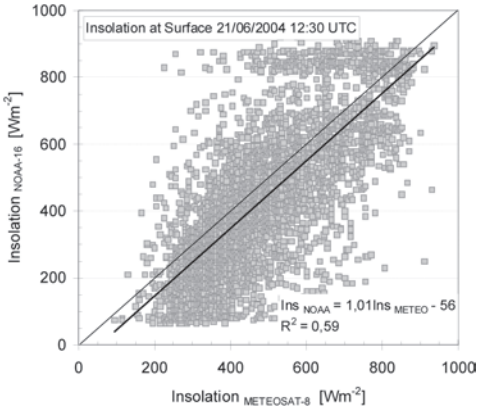

Fig. 8: Inter satellite comparison of insolation at surface for 21/06/2004, 12:30 UTC for the area 15–25°E, 50–55°N with thicker and high clouds dominating.

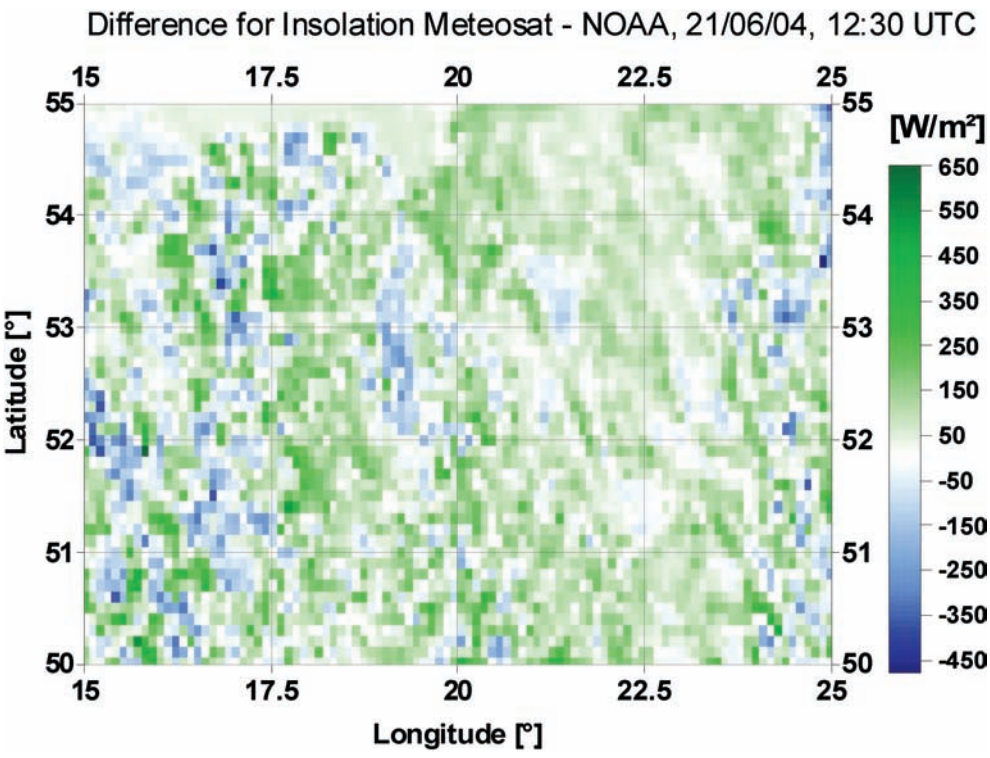

Fig. 9: Difference Plot of insolation for the above defined area.

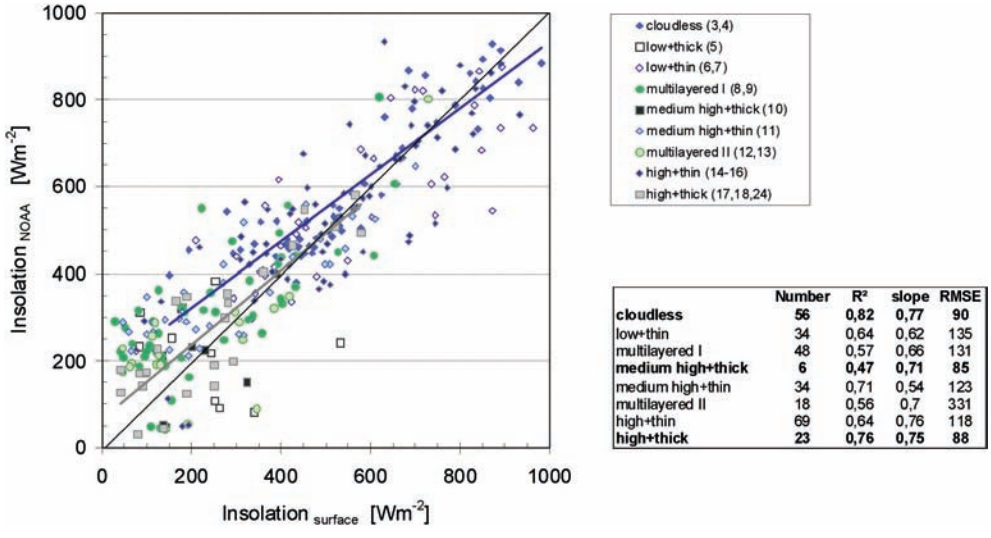

	Number	R^2	slope	RMSE
cloudless	**56**	**0,82**	**0,77**	**90**
low+thin	34	0,64	0,62	135
multilayered I	48	0,57	0,66	131
medium high+thick	**6**	**0,47**	**0,71**	**85**
medium high+thin	34	0,71	0,54	123
multilayered II	18	0,56	0,7	331
high+thin	69	0,64	0,76	118
high+thick	**23**	**0,76**	**0,75**	**88**

Fig. 10: Validation of the NOAA insolation results with half-hourly ground measurements at 3 Anchor Stations in eastern Germany.

types as well as cloudless features (see box). Thinner clouds with optical thickness < 10 often show inhomogeneous structures which leads to greater uncertainties for the determination of insolation. Multilayered clouds are hard to parameterize due to lack of information about 3D cloud field and vertical structure. The RMSE therefore is much higher here. The accuracy of ground measurements of insolation usually is assumed to be $\pm$ 3 % for class A pyranometers. The variation within the 10×10 pixel mean is higher depending on the respective cloud structure. However, the NOAA geocoding has a limited accuracy, so the use of a pixel mean is highly recommended, if no second navigation is applied. Another problem: the instantaneous satellite data are compared with half-hourly data. Even with interpolation one may not meet the appropriate value especially for temporally high variable quantities.

5 Discussion

The results clearly show the deficits within the cloud parameterization especially for Meteosat. The adjustments of SESAT to Meteosat were tested with one scene only, so the results are still preliminary. Further testing for time series is required to improve the adaptation. The application of the high resolution visible (HRV) channel of Meteosat-8 with a resolution of 1 km at nadir would solve certain problems which are explicitly related to the coarser resolution currently used. Due to the short period of Metesosat-8 data availability no examination of measurement (sensor) uncertainties was carried out so far. The evaluation has to be extended towards more cloud types to further discuss the effect of different clouds on radiative transfer. Recently generated look-up tables (Streamer) which include bidirectional reflection functions for land surfaces and clouds instead of assuming isotropic conditions will enhance the accuracy of radiation and improve the quality of cloud properties.

The obtained accuracies for insolation are within the range of other investigations showing validation with ground truth data for instantaneous quantities (RMSE about 120 Wm^{-2}). The uncertainty of both NOAA and Metosat-8 results has to be accounted for in follow-up computations. The quality of insolation results is sufficient for monthly data but for instantaneous data the accuracy is still limited.

Acknowledgements

The ground measurement data used for validation were collected within the BMBF research programme AFO 2000 through TU Dresden (IHM), DWD (Observatorium Lindenberg) and Institut für Troposphärenforschung Leipzig.

References

Berger, F. H., 1995: Inference of the climate efficiency of clouds from satellite measurements. – Int. J. Remote Sensing **16** (15): 2903–2926.

Berger, F. H., 2001: Bestimmung des Energiehaushaltes am Erdboden mit Hilfe von Satellitendaten. – Tharandter Klimaprotokolle, Band 5.

Berger, F. H., Ackermann, J. & Klaes, D., 2002: Surface radiant flux densities inferred from LAC and GAC AVHRR data. – Proceedings of "The Eumetsat User's Conference", Dublin September 2002.

Chou, M.-D., Suarez, M. J., Ho, C.-H., Yan, M. M.-H. & Lee, K.-T., 1997: Parameterizations for cloud overlapping and shortwave single-scattering properties for use in general circulation and cloud ensemble models. – J. Clim. **11:** 202–214.

Eumetsat, 2003: Image Data Dissemination Service, Technical Description EUM TD 08, p. 16.

Key, J. R., 1999: Streamer – user's guide, Technical Report 96–01, Department of Geography, Boston University.

Laszlo, I. & Pinker, R. T., 1993: Shortwave cloud-radiative forcing at the top of the atmospere, at the surface and of the atmospheric column as determined from ISCCP C1 data. – J. Geoph. Res. **98:** 2703–2713.

Masuda, K., Leighton, H. G. & Li, Z., 1995: A new parameterization for the determination of solar flux absorbed at the surface from satellite measurements. – J. Clim. **8:** 1615–1629.

McClain, E. P., Pichel, W. G. & Walton, C. C., 1985: Comparative performance of AVHRR-

based multichannel sea surface temperatures. – J. Geophys. Res. **90:** 11587–11601.

NOAA KLM User's Guide, September 2000 Revision.

Pincus, R., Szczodrak, M., Gu, J., Austin, P., 1995: Uncertainty in cloud optical depth estimates made from satellite radiance measurements. – J. Clim. **8:** 1453–1462.

Pinker, R. T., Frouin, R. & Li, Z., 1995: A review of satellite methods to derive surface shortwave irradiance. – Remote Sens. Environ. **51:** 108–124.

Rozwadowska, A., 2004: Uncertainty in stratiform cloud optical thickness inferred from pyranometer measurements at the sea surface. – *Oceanologia* **46:** 155–174.

Schmetz, J., 1993: Relationship between solar net radiative fluxes at the top of atmosphere and at surface. – J. Atm. Sci. **50:** 1122–1132.

Schwiebus, A. & Berger, F.H., 2004 (in press): Sensitivity studies and their application to infer surface energy fluxes: prospects within the passive remote sensing. – Physics and Chemistry of the Earth.

Song, J. & Gao, W., 1999: An improved method to derive surface albedo from narrowband AVHRR satellite data: Narrowband to broadband conversion. – J. Appl. Meteor. **38:** 239–249.

Tarpley, J. D., 1979: Estimating incident solar radiation at the surface from geostationary satellite data. – J. Appl. Meteor. **18:** 1172–1181.

Taylor, D., 2003: http://www.david-taylor.pwp.blueyonder.co.uk/software/

Tovar, H. F. & Baldasano, J. M., 2001: Solar radiation mapping from NOAA AVHRR data in Catalonia, Spain. – J. Appl. Meteor. **40:** 1821–1834.

Yucel, I., Shuttleworth, W. J., Pinker, R. T., Lu, L. & Sorooshian, S., 2002: Impact of ingesting satellite-derived cloud cover into the regional atmosheric modeling system. Mon. Weather Rev. **130:** 610–628.

Addresses of the authors:

Angela Schwiebus
e-mail: angela.schwiebus@forst.tu-dresden.de

Anne Lorenz
e-mail: anne.lorenz@forst.tu-dresden.de
Anschrift:
TU Dresden
Institut für Hydrologie und Meteorologie
LS Meteorologie
D-01062 Dresden

PD Mag. Dr. Franz H. Berger
e-mail: franz.berger@dwd.de
Anschrift:
Deutscher Wetterdienst
Meteorologisches Observatorium Lindenberg
D-15848 Tauche – OT Lindenberg

Manuskript eingereicht: Oktober 2004
Angenommen: November 2004